Nonstoichiometric $La_{2-x}GeO_{5-\delta}$ Monoclinic Oxide as a New Fast Oxide Ion Conductor

Tatsumi Ishihara,* Hiroshi Arikawa, Taner Akbay, Hiroyasu Nishiguchi,* and Yusaku Takita*

Contribution from the Department of Applied Chemistry, Faculty of Engineering, Oita University, Dannoharu 700, Oita 870-1192, Japan

Received April 26, 2000

Abstract: Oxide ion conductivity in La_2GeO_5-based oxide was investigated and it was found that La-deficient La_2GeO_5 exhibits oxide ion conductivity over a wide range of oxygen partial pressure. The crystal structure of La_2GeO_5 was estimated to be monoclinic with $P2_1/c$ space group. Conductivity increased with increasing the amount of La deficiency and the maximum value was attained at $x = 0.39$ in $La_{2-x}GeO_{5-\delta}$. The oxide ion transport number in La_2GeO_5-based oxide was estimated to be unity by the electromotive force measurement in H_2-O_2 and N_2-O_2 gas concentration cells. At a temperature higher than 1000 K, the oxide ion conductivity of $La_{1.61}GeO_{5-\delta}$ was almost the same as that of $La_{0.9}Sr_{0.1}Ga_{0.8}Mg_{0.2}O_{3-\delta}$ or $Ce_{0.85}Gd_{0.15}O_{2-\delta}$, which are well-known fast oxide ion conductors. On the other hand, a change in the activation energy for oxide ion conductivity was observed at 973 K, and at intermediate temperature, the oxide ion conductivity of $La_{1.61}GeO_{5-\delta}$ became much smaller than that of these well-known fast oxide ion conductors. The change in the activation energy of the oxide ion conductivity seems to be caused by a change in the local oxygen vacancy structure. However, doping a small amount of Sr for La in La_2GeO_5 was effective to stabilize the high-temperature crystal structure to low temperature. Consequently, doping a small amount of Sr increases the oxide ion conductivity of La_2GeO_5-based oxide at low temperature.

Introduction

Oxide ion conductors are eminent materials that take an integral part in a number of applications, e.g. fuel cells, oxygen sensors, and oxygen separating membranes. An oxygen sensor is essential for combustion control and a fuel cell is expected to be a new and clean electric power source, in particular, for electric vehicles. An oxygen-separating film is expected to be a potable and economical oxygen source for medicine and catalytic oxidative processes. So far, tetravalent oxides with fluorite structures such as ZrO_2 and CeO_2 are widely utilized as the oxide ion conductor in various applications.[1,2] In addition, there are reports on fast oxide ion conductivity in oxides with nonfluorite crystal structures too.[3,4] Furthermore, it should be noted that an integral portion of known fast oxide ion conductors possess either cubic or pseudocubic crystal lattices. Discovery of $LaGaO_3$ with a pseudocubic perovskite lattice by the authors was not an exception to the above-mentioned fact.[5−8] Therefore, it is generally believed that high symmetry in a crystal lattice is an essential requirement for depicting the fast oxide ion conducting property. So far there have been a limited number of reports in the literature on the notable oxide ion conductivity in noncubic structured oxides. Among the few exceptions, the oxide ion conductivity in hexagonal appetite oxide of $La_{10}Si_6O_{27}$ and $Nd_{10}Si_6O_{27}$ reported by Nakayama et al.[9,10] is highly interesting. However, the oxide ionic conductivity values of these oxides at elevated temperatures (higher than 873 K) were not high enough compared with that of the conventional oxide ion conductors. On the other hand, the bismuth-based oxide of BIMEVOX,[11] Aurivillius phase ($Bi_2A_{n-1}B_nO_{3n+1}$, $n = 1-5$),[12] and δ-Bi_2O_3 are reported as the high oxide ion conductor with noncubic or pseudocubic structure, respectively; however, this oxide exhibited wholly oxide ionic conductivity in a limited P_{O_2} range.[11,12] In the present investigation, the authors would like to report the notably high oxide ion conducting property of La_2GeO_5-based oxide with monoclinic lattice. Since it is expected that oxide ion can move more easily in the crystal lattice with increasing the lattice volume, the high oxide ionic conduction is expected on La_2GeO_5, which has a larger unit volume than that of $La_{10}Si_6O_{27}$ oxide.

Experimental Section

Conventional powder mixing methods were always utilized to prepare all specimens in this investigation. Commercially available La_2O_3 (Kishida 99.99%), $SrCO_3$ (Wako, 99.9%), and GeO_2 (Nakarai 99.99%) powders were mixed in varying proportions to obtain a range in composition of $La_{2-x}GeO_{5-\delta}$. The starting batch was mixed in an

* Address correspondence to this author.

(1) Choudhary, C. B.; Maiti, H. S.; Subbarao, E. C. *Solid Electrolytes and Their Applications*; Subbarao, E. C.; Planum: New York, 1980; p 1.
(2) Steele, B. C. H. *J. Power Source* **1994**, *49*, 1.
(3) Takahashi, T.; Iwahara, H. *Energy Conversion* **1971**, *11*, 105.
(4) Kendall, K. R.; Navas, C.; Thomas, J. K.; zur Loye, H. C. *Solid State Ionics* **1995**, *82*, 215.
(5) Ishihara, T.; Matsuda, H.; Takita, Y. *Solid State Ionics* **1995**, *79*, 147.
(6) Ishihara, T.; Kilner, J. A.; Honda, M.; Takita, Y. *J. Am. Chem. Soc.* **1997**, *119*, 2747
(7) Ishihara, T.; Matsuda, H.; Takita, Y. *J. Am. Chem. Soc.* **1998**, *116*, 3801.
(8) Slater, P. R.; Irvine, J. T. S.; Ishihara, T.; Takita, Y. *J. Solid State Chem.* **1998**, *139*, 135.
(9) Nakayama, S.; Sakamoto, M. *J. Euro. Ceram. Soc.* **1998**, *18*, 1413.
(10) Nakayama, S. *Mater. Integration* **1999**, *12* (4), 57.
(11) Abraham, F.; Boivin, J. C.; Mairesse, G.; Nowogrocki, G. *Solid State Ionics* **1990**, *40−41*, 934.
(12) Kendal, K. R.; Navas, C.; Thomas, J. K.; Loye H. C. *Chem. Mater.* **1996**, *8*, 642.

10.1021/ja0014537 CCC: $20.00
Published on Web 12/15/2000

Al_2O_3 mortar with a pestle followed by a precalcination at 1273 K for 6 h. The mixture was pressed into disks of 20-mm diameter followed by sintering in air at 1923 K for 6 h.

Cu Kα radiation was used to perform the powder X-ray diffraction (XRD) measurements by a diffractometer (Rigaku Rint 2500). The crystal structure of the sample was analyzed by using the Rietveld method with Rietan 98. The apparent density of the resultant La_2GeO_5, estimated by Archimedes method, was 5. 52 g/cm^3, which is ca. 95% of the theoretical value (5.874 g/cm^3). Therefore, the sintering property of La_2GeO_5 is essential in obtaining a highly dense sample. The thermal expansion property was measured in a N_2 gas flow by a thermal mechanical analyzer (TMA, Rigaku Thermoplus 8310) to analyze the phase change of the local structure. A sintered sample of $La_{1.61}GeO_{5-\delta}$ was cut into a rectangular shape ($2 \times 2 \times 5$ mm^3) and heated to 1273 K at the rate of 10 K/min for TMA measurement. The scanning electron microscopy (SEM) observation was performed with an Hitachi S-2400 which was equipped with an X-ray fluorescence analyzer (Horiba, EMAX-2770). X-ray images of La and Ge were obtained by using the Lα line and Sr by using the Kα line.

Oxide ionic conductivity was measured by a conventional ac two-probe technique with a frequency response analyzer (Solatron 1260) in a frequency range from 10 MHz to 1 Hz. Commercial platinum paste (Tanaka, TR7902) was applied on both faces of the sample followed by calcination at 1173 K for 30 min. Two semicircles, which can be assigned to the bulk conductivity and the electrode overpotential, were always observed in the complex impedance plane plots of the specimens. Resistance of the sample was estimated with the resistance sectioned by the first semicircle appearing in a high-frequency range. Conductivity was also measured with the dc four-probe method and it is also noted that the conductivity estimated by both methods was matched within a small error. Therefore, the estimated conductivity is considered to be accurate and reproducible. Accordingly, error bars for oxide ion conductivity are omitted. A gas flow cell was designed to perform the oxide ionic conductivity measurements under the controlled atmosphere maintained by using mixtures of N_2-O_2, $CO-CO_2$, and H_2-H_2O. The oxygen partial pressure was monitored by using a CaO-stabilized ZrO_2 oxygen sensor placed in close proximity of the specimens. The transport number of the oxide ion was estimated by the ratio of measured electromotive forces in the H_2-O_2 and N_2-O_2 gas concentration cell to that estimated with Nernst equation. Oxide ion diffusivity was further measured with the ^{18}O tracer diffusion measurement. The polished specimens were annealed in $^{18}O_2$ (95%) at 1073 K for 900 s followed by measuring with secondary ion mass spectroscopy (ATOMIKA 4100) with Cs^+ (accelerate voltage of 15 kV) as a primary ion source. Details are described elsewhere.[13]

Results and Discussion

Crystal Structure of La-Deficient La_2GeO_5 Oxide. Results of the XRD measurements of $La_{2-x}GeO_{5-\delta}$ are shown in Figure 1. It should be noted that the single phase of the La_2GeO_5 crystal structure was maintained up to the value of $x < 0.45$ in $La_{2-x}GeO_{5-\delta}$. This observation suggests that La_2GeO_5 can accommodate a large amount of La deficiency without the appearance of secondary phases. Although there has been no detailed analysis of the crystal structure of La_2GeO_5 in the literature, the crystal lattice of Ln_2GeO_5 (Ln = lanthanide) was identified as a monoclinic lattice by referring to the JCPDS database[14,15] and ICSD database of Gd_2GeO_5.[16] From now on in this manuscript, the crystal structure of the specimens with La-deficiency $x < 0.39$ will be referred to as monoclinic. La-deficiencies $x > 0.45$, however, resulted in a distinct phase transformation in $La_{2-x}GeO_{5-\delta}$, which was suggested by the introduction of extra diffraction peaks and broadening of the existing ones in the XRD pattern (Figure 1). At $x = 0.39$,

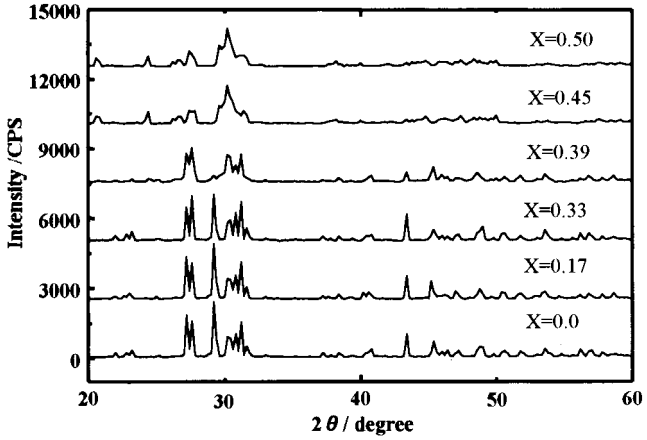

Figure 1. X-ray diffraction patterns of $La_{2-x}GeO_{5-\delta}$ at room temperature.

diffraction patterns began to broaden; however, the typical diffraction pattern of non-La-deficient La_2GeO_5 was observed, in particular, around the main peak. Accordingly, it seems likely that the monoclinic structure of $P2_1/c$ was the main phase in $La_{1.61}GeO_{5-\delta}$. Although the diffraction patterns were changed, there exists some similarity in XRD patterns between the that of the newly appearing crystal structure and the original one of the La_2GeO_5 peaks around $2\theta = 23°$. It is clear that XRD patterns of the samples, in particular, the sample with La deficiency $x \leq 0.33$, were well fitted as the monoclinic lattice with space group $P2_1/c$. On the other hand, XRD patterns of sample with $x \geq 0.45$ were the most fitted with the $P2_1$ space group which is further distorted from $P2_1/c$, although a similar pattern cannot be found in any crystallographic database. However, deviation of the fitting data from the measured pattern was still large and the crystal structure of this $P2_1$ phase is under investigation in greater detail.

Phase separation was also investigated by secondary electron microscopy (SEM) with the X-ray fluorescence analyzer. Figure 2 shows an SEM photograph and X-ray images of La and Ge in $La_{1.61}GeO_{5-\delta}$. SEM observation suggests the resultant sample was dense and no large pore was observed. An X-ray image of the La and Ge Lα line suggests that the distribution of La and Ge was completely uniform and no segregation of La or Ge was observed. Therefore, it is obvious that the formation of a secondary phase or segregation of the component element was negligible in the resultant specimens.

Table 1 summarizes the atomic position of La^{3+}, Ge^{4+}, and O^{2-} in $La_{2-x}GeO_5$ with $P2_1/c$ estimated by Rietveld analysis. Although a large amount of La deficiency was introduced, the atomic position of La^{3+}, Ge^{4+}, and O^{2-} was not significantly changed. Therefore, despite La deficiency, the crystal structure was stably sustained. On the other hand, some similarity was observed in diffraction patterns of samples at $x < 0.45$ and those at $x > 0.45$. Therefore, the crystal structure of $P2_1$ seems to have some similarity with those of $P2_1/c$, albeit further detailed study on the crystal structure with $P2_1$ was required. Table 2 summarizes the refined lattice parameters obtained by Rietveld analysis for the $P2_1/c$ phase. This La-deficient La_2GeO_5 has a slightly longer *a*-axis lattice parameter than that of *b* and *c*. It is also noted that the unit volume size gradually decreased with an increase in the La-deficient amount. This may be related to the increase in oxygen deficiency. The crystal structure of La_2GeO_5 ($P2_1/c$ phase) fitted with Rietveld analysis is schematically shown in Figure 3. The crystal lattice of $La_{2-x}GeO_{5-\delta}$ consists of large La^{3+} and O^{2-} ions and small ions of Ge^{4+} located in the central position of the triangular prism in Figure 3. From

(13) Manning, P. S.; Sirmon, J. D.; Kilner, J. A. *Solid State Ionics* **1997**, *93*, 125.
(14) JCPDS-International Center for Diffraction Data, No. 40-1183.
(15) JCPDS-International Center for Diffraction Data, No. 76-694.
(16) ICDS Collection Code 61372.

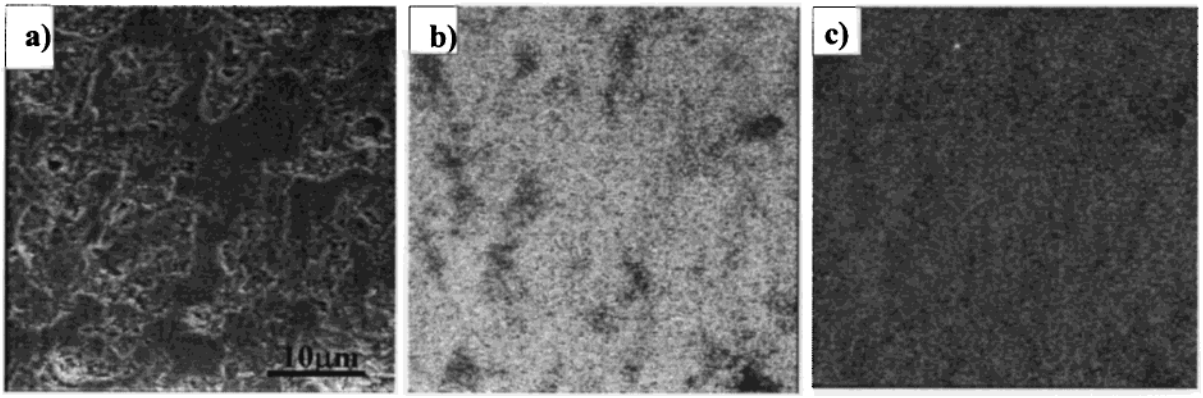

Figure 2. SEM photograph and X-ray image of the La and Ge Lα line in $La_{1.61}GeO_{5-\delta}$: (a) SEM photograph, (b) X-ray image of the La Lα line, and (c) X-ray image of the Ge Lα line.

Table 1. Refined Atomic Coordinate in $La_{2-x}GeO_{5-\delta}$ with $P2_1/c$ Estimated by the Rietveld Method

atomic coordinate	occupancy	*X*	*Y*	*Z*
La(1)				
$x = 0.00$	1.000	0.38937	0.14161	0.57941
$x = 0.17$	0.917	0.38314	0.14551	0.58269
$x = 0.33$	0.833	0.38243	0.13816	0.58078
La(2)				
$x = 0.00$	1.000	0.02056	0.12360	0.72966
$x = 0.17$	0.917	0.02089	0.12454	0.73322
$x = 0.33$	0.833	0.02073	0.12401	0.72818
Ge				
$x = 0.00$	1.000	0.29732	0.58935	0.53976
$x = 0.17$	1.000	0.29377	0.58450	0.54373
$x = 0.33$	1.000	0.30041	0.58445	0.54512
O(1)				
$x = 0.00$	1.000	0.32250	0.06691	0.86216
$x = 0.17$	0.950	0.30619	0.05003	0.85943
$x = 0.33$	0.900	0.30359	0.05100	0.86660
O (2)				
$x = 0.00$	1.000	0.34794	0.48623	0.75895
$x = 0.17$	0.950	0.39602	0.45698	0.77947
$x = 0.33$	0.900	0.40928	0.31364	0.79364
O (3)				
$x = 0.00$	1.000	0.35157	0.77243	0.49523
$x = 0.17$	0.950	0.34462	0.73855	0.49488
$x = 0.33$	0.900	0.34575	0.76911	0.51233
O (4)				
$x = 0.00$	1.000	0.04677	0.61215	0.49451
$x = 0.17$	0.950	0.05107	0.62272	0.49309
$x = 0.33$	0.900	0.04304	0.67208	0.47461
O (5)				
$x = 0.00$	1.000	0.04310	0.12912	0.45330
$x = 0.17$	0.950	0.08703	0.07450	0.44707
$x = 0.33$	0.900	0.07236	0.11107	0.43257

Table 2. Refined Lattice Parameter of La_2GeO_5-Based Oxide with $P2_1/c$ Obtained by the Rietveld Method

$La_{2-x}GeO_{5-\delta}$ standard dev. $x =$	lattice parameter/pm *a*	*b*	*c*	angle/deg. β	cell vol. $\times 10^6$ pm^3	R.wp*
0.00	959.693	747.359	710.745	107.5770	485.97	11.74
	0.00078	0.00050	0.00054	0.0049		9.39
0.17	959.792	747.129	710.810	107.5631	485.95	12.80
	0.00084	0.00055	0.00059	0.0052		9.63
0.33	9.60248	748.187	711.235	107.5695	487.15	14.32
	0.00097	0.00064	0.00068	0.0060		11.27

* R factors.

the point of view of oxygen, La_2GeO_5 consisted of two types of oxygen: one is four oxygens covalently bonded to Ge to form GeO_4 tetrahedral units and the other is one oxygen which is bridged between La^{3+} and GeO_4^{4-} tetrahedral units. Figure 3b is the crystal structure for further larger units from the *c*-axis direction, (001). It is obvious that La_2GeO_5 consists of two kinds of layers, i.e., one is the double layers of lanthanum, germanium, and oxygen and the other is the monolayer of La^{3+} and O^{2-} between the La−Ge−O layer. Therefore, it is obvious that there is a great anisotropy in oxygen structure exists in this La_2GeO_5 crystal. It is also noted that coordination numbers of La and Ge in this structure are 6 and 4, respectively.

The high-temperature XRD pattern of La_2GeO_5 is further measured to confirm the stability of the crystal lattice. Figure 4 shows XRD patterns of $La_{1.67}GeO_{5-\delta}$ at elevated temperature. Further detailed diffraction patterns around 30° are also shown in Figure 4b. It is clear that the increase in temperature causes the broadening diffraction peaks and shift to a lower diffraction angle as shown in Figure 4b. This is caused by the thermal expansion of the lattice. It is also noted that X-ray diffraction peaks from the Pt heater were observed in Figure 4a and the intensity of these peaks was changed with temperature, since the Pt heater line seems to vibrate slightly by applying the electric power. However, it should be noted that the identification of peaks for the high-temperature analysis was exactly the same as that at room temperature. This suggests that the monoclinic structure shown in Figure 3 remains stably up to 1273 K and no significant phase change in a long-range order occurred up to 1273 K.

Phase stability of La-deficient La_2GeO_5 was further studied with thermal mechanical analysis (TMA) measurement. Figure 5 shows the thermal expansion property of $La_{1.67}GeO_{5-\delta}$. It is obvious that the thermal expansion property exhibited a large curvature at 973 K. The average thermal expansion coefficient changed from 8.8×10^{-6} (473−873 K) to 12.4×10^{-6} K^{-1} (1073−1273 K). This suggests that some crystal structure changed around 973 K. Considering no clear change in XRD patters at elevated temperature as shown in Figure 4, the local structure in a short range may have changed around 973 K. This local structure change reflected the order−disorder change in the oxygen vacancy structure.

Oxide Ion Conductivity in La-Deficient La_2GeO_5 Oxide. Figure 6 shows the Arrhenius plots of the total conductivity values measured in $La_{2-x}GeO_{5-\delta}$. It is obvious that La_2GeO_5 ($x = 0$) is not a good conductor; total conductivity is lower than $\log(\sigma/\mathrm{S\ cm^{-1}}) = -4$ at all temperatures. However, the total conductivity increased with increasing the amount of La deficiency and it reached a maximum at $x = 0.39$ at temperatures higher than 1073 K. Referring to the XRD observations, the phase transformation at about the same La deficiency may cause the decrease in the total conductivity as seen in Figure 6. Therefore, it is safe to conclude that the highest total conductivity can be achieved by the largest La deficiency in the single

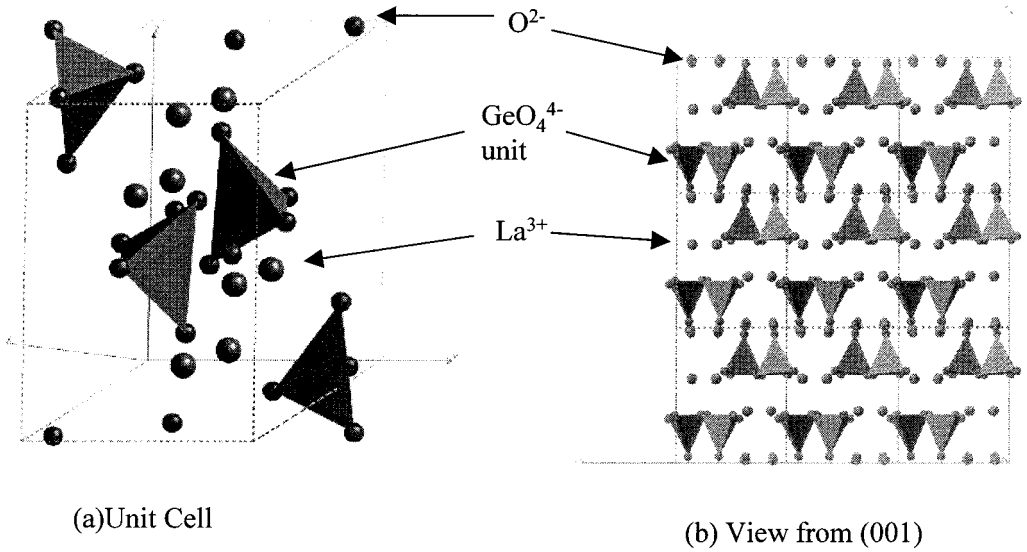

Figure 3. Crystallographic view of $La_{2-x}GeO_{5-\delta}$ structure: (a) unit cell and (b) view from the (001) direction.

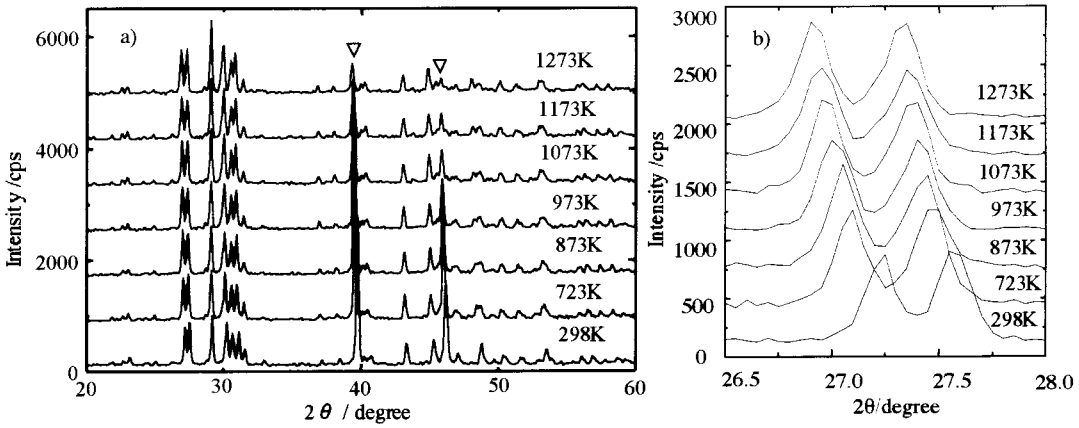

Figure 4. XRD patterns of $La_{1.67}GeO_5$ at elevated temperature in air: (a) wide diffraction angle and (b) magnification around main peak; ∇ = Pt.

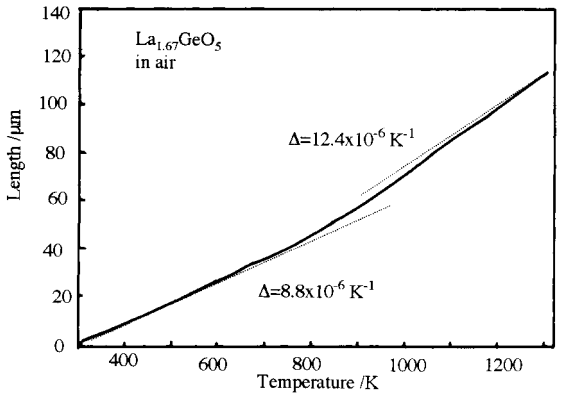

Figure 5. Thermal expansion property of $La_{1.67}GeO_{5-\delta}$ in air. The heating rate = 10 K/min.

monoclinic structure of $La_{2-x}GeO_{5-\delta}$ with the $P2_1/c$ space group. However, the difference in the total conductivity at temperatures higher than 1073 K was not significant between the samples in $x = 0.33-0.39$. This may suggest the saturation of the oxygen defect and the association between oxygen and cation defects seems to occur, which is related to the phase transformation from $P2_1/c$ to $P2_1$. It also should be noted that the slope of the Arrhenius plots changed at 973 K in the case of La-deficient La_2GeO_5. The estimated activation energies for the total conductivity in $La_{1.61}GeO_{5-\delta}$ at high and low temperature were 0.858 ± 0.01 and 1.702 ± 0.02 eV, respectively.

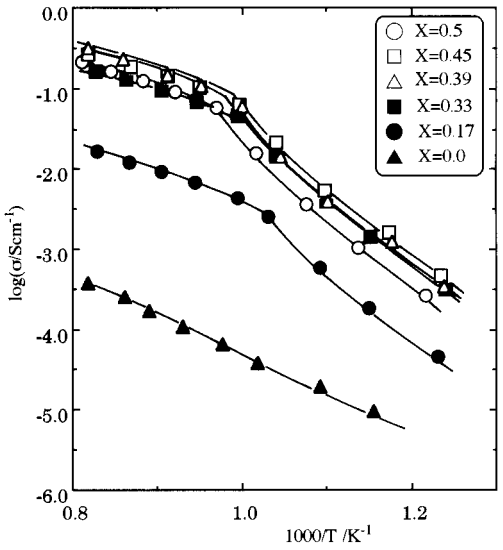

Figure 6. Ahrrenius plots of the total conductivity of $La_{2-x}GeO_{5-\delta}$ in $P_{O_2} = 10^{-5}$ atm.

This behavior can be explained by referring to an order−disorder transition in oxygen vacancy structure in the local structure, which is suggested by the thermal expansion property. At temperatures lower than 1073 K, the maximum total conductivity was attained at $x = 0.45$. This may suggest that the limit concentration of oxygen vacancy for the association varies in

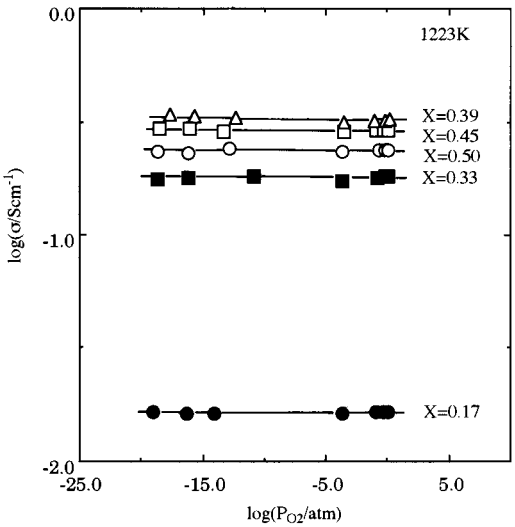

Figure 7. Total conductivity of $La_{2-x}GeO_{5-\delta}$ at 1173 K as a function of oxygen partial pressure.

the oxygen ordered and disordered structure. In any case, the high total conductivity was exhibited on the specimens at La deficiency $0.33 < x < 0.45$.

The total conductivity of $La_{2-x}GeO_{5-\delta}$ at 1223 K as a function of oxygen partial pressure is shown in Figure 7. It is well-known that total conductivity of n- and p-type semiconductor increases and decreases as the oxygen partial pressure increases, respectively. On the other hand, total conductivity is independent of the oxygen partial pressure when the ion conductivity is dominant. Therefore, total conductivity as a function of oxygen partial pressure gives information on the main charge carrier in oxides. It is self-evident that all specimens exhibit the total conductivity, which is independent of the oxygen partial pressure in a wide P_{O_2} range. The constant total conductivity of $La_{2-x}GeO_{5-\delta}$ over a wide range of oxygen partial pressures ($P_{O_2} = 1.0$ to 10^{-19} atm) is strong evidence for the dominant oxide ion conductivity in this particular oxide.

Oxide ion transport numbers can be estimated by using electromotive forces obtained from the oxygen gas concentration cell. If the oxide ion is the only charge carrier in the specimens, then the electromotive forces should obey the Nernst equation. By using this argument, the transport number of oxide ion conductivity can be approximately estimated by calculating the ratio of the measured electromotive forces to those estimated from the Nernst relation. Figure 8 depicts the temperature dependence of the oxide ion transport number in $La_{1.61}GeO_{5-\delta}$ calculated by using the electromotive forces in the H_2-O_2 and N_2-O_2 gas concentration cell. It is clear that $La_{1.61}GeO_{5-\delta}$ exhibits almost the theoretical electromotive force value in both H_2-O_2 and N_2-O_2 cells. This suggests that oxide ion conductivity in $La_{1.61}GeO_{5-\delta}$ is stable over a wide oxygen partial pressure from oxygen to hydrogen. The estimated oxide ion transport number always remains higher than 0.98 (less than 10 mV deviation from the theoretical value) at temperature from 873 to 1273 K. Even considering the experimental errors in electromotive force measurements, it can be said that the total conductivity of La-deficient La_2GeO_5 is wholly ionic.

Oxygen tracer diffusion measurement is the reliable technique to confirm the oxide ion conductivity in oxide.[6,13,17,18] The diffusion property of oxygen into the $La_{1.61}GeO_{5-\delta}$ lattice was further studied with the ^{18}O tracer diffusion measurement by

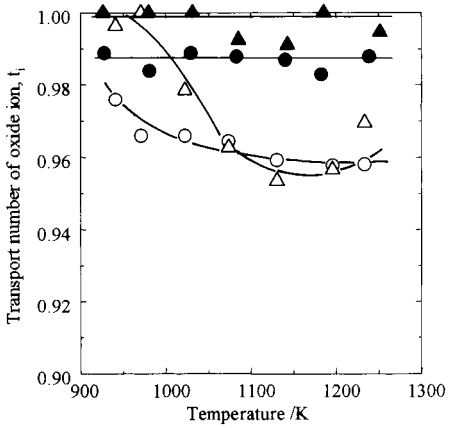

Figure 8. Temperature dependence of the transport number of oxide ion in $La_{1.67}GeO_{5-\delta}$ and $La_{1.5}Sr_{0.17}GeO_{5-\delta}$. Transport number in $La_{1.67}GeO_{5-\delta}$: (○) H_2-O_2 cell and (△) N_2-O_2 cell. Transport number in $La_{1.5}Sr_{0.17}GeO_{5-\delta}$: (●) H_2-O_2 cell and (▲) N_2-O_2 cell.

secondary ion mass spectroscopy (SIMS). The enrichment part of the ^{18}O in bulk, which was independent of the grain boundary, was observed in the sample and this might be result from the large anisotropy in the oxide ion diffusivity, which was caused by the anisotropy in the crystal structure as shown in Figure 3b. In response with the anomalous enrichment of ^{18}O, the deviation part was observed on a diffusion curve of ^{18}O. However, it is considered that the obtained diffusion curve of ^{18}O can be well fitted to the diffusion equation considering a surface exchange reaction[13] excepting the deviation part. Therefore, the estimated diffusion and the surface exchange coefficient seem not to be strongly influenced by the anomalous diffusion of oxygen, albeit a small error may be contained in the estimated values. The estimated self-diffusion and surface exchange coefficient were 1.76×10^{-7} cm^2/s and 6.88×10^{-7} cm/s, respectively, at 923 K. The diffusion coefficient almost corresponded to a value (1.90×10^{-7} cm^2/s) estimated by the total conductivity and the Nernst−Einstein equation. Considering the experimental errors in electromotive force and tracer diffusion measurement, it can be concluded that the total conductivity of La-deficient La_2GeO_5 is wholly ionic. Currently, it was speculated that oxide ion diffusion mainly occurred along the (011) plane through a layer consisting of La and O, since oxygen bonded to Ge is strongly held. In any case, there is substantial evidence for improved oxide ion conductivity when a certain amount of La deficiency was introduced into La_2GeO_5. Therefore, oxide ion might move around the lattice through the oxygen vacancy formed by the Schottky-type defect which was formed by the following equation expressed with Kröger−Vink notification

$$La_{La}^{\ x} + {}^3/_2O_O^{\ x} = V_{La}''' + {}^3/_4O_2 + {}^3/_2V_O^{\bullet\bullet} + La_S^{\ x}$$

where $V_O^{\bullet\bullet}$ and S are the oxygen vacancy and the surface sites, respectively. Since the number of charge carriers increases with increasing La deficiency, the oxide ion conductivity will increase with increasing the amount of La-deficiency. However, there is an apparent limit to the amount of La-deficiency as the crystal structure transforms from the monoclinic to the distorted monoclinic structure when La deficiency becames excess.

Figure 9 shows the comparison of oxide ion conductivity of $La_{1.61}GeO_{5-\delta}$ with that of fluorite and perovskite structured oxides. The comparison clearly reveals that at temperatures higher than 1000 K, the oxide ion conductivity of $La_{1.61}GeO_{5-\delta}$ is much higher than that of Y_2O_3-stabilized ZrO_2 and it is almost

(17) Manning, P. S.; Sirman, J. D.; Kilner, J. A. *Solid State Ionics* **1997**, *93*, 125.

(18) Sirman, J. D.; Kilner, J. A. *J. Electrochem. Soc.* **1996**, *143*, L229.

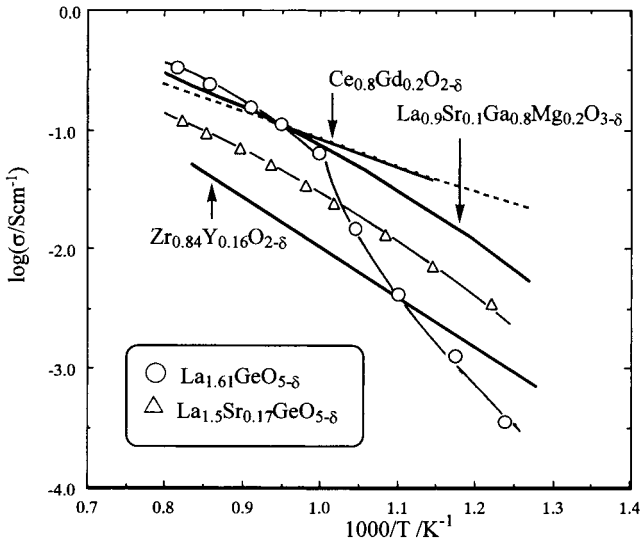

Figure 9. Comparison of the oxide ion conductivity in $La_{1.61}GeO_{5-\delta}$ and $La_{1.5}Sr_{0.17}GeO_{5-\delta}$ with those of the conventional oxide ion conductors.

the same as that of CeO_2 doped with Gd_2O_3 (GDC) or $La_{0.9}Sr_{0.1}Ga_{0.8}Mg_{0.2}O_3$ (LSGM). However, at low temperature, the oxide ion conductivity of $La_{1.61}GeO_{5-\delta}$ is much smaller than that of rest as a result of the change in activation energy. From the high ionic conductivity point of view, La-deficient La_2GeO_5 oxide is an attractive material at high temperature; however, the activation energy for oxide ion conductivity is changed around 973 K and the oxide ion conductivity at low temperature becames smaller than that of the conventional oxide ion conductor. Therefore, an increase in oxide ion conductivity at low temperature is further required.

Effects of Sr Doped for the La Site in $La_{1.67}GeO_{5-\delta}$. It is well-known that doping a small amount of lower valence cation forms an oxygen vacancy, which increases the oxide ion conductivity. It is also noted that such a lower valence cation sometimes stabilizes the high-temperature structure to low temperature. Cubic ZrO_2 is the typical case of this stabilization effect. In this work, the dopant effect on the oxide ion conduction of La_2GeO_5 at low temperatures was further investigated. A slightly small La-deficiency ($x = 0.33$) was chosen for this purpose since this composition exists in the monoclinic region of the phase diagram as shown in Figure 2. An XRD measurement of Sr-doped $La_{1.67}GeO_{5-\delta}$-based oxide was also performed and it became clear that diffraction pattern of Sr-doped La_2GeO_5-based oxide was the same as that of parent La_2GeO_5 with a $P2_1/c$ space group and no peaks from secondary phase were observed. Therefore, it is considered that Sr was substituted into the lattice position of La in the La_2GeO_5 lattice. It is also noted that change in the lattice parameter was hardly observed because the ionic radius of six-coordinated Sr^{2+} is almost the same as that of La^{3+}.[19]

Since the dopant level of Sr is low, phase separation of Sr was also investigated by SEM observation and X-ray fluorescence analysis. Figure 10 shows an SEM photograph and X-ray images of La, Sr, and Ge in $La_{1.5}Sr_{0.17}GeO_{5-\delta}$. SEM observation suggests the resultant Sr-doped sample was also dense, which is the same as that of the La-deficient sample. On the other hand, the X-ray image of the La and Ge Lα and Sr Kα lines suggests that the distribution of La, Sr, and Ge was completely uniform. Considering no diffraction peak assigned to a secondary phase observed in XRD patterns, it could be said that the

(19) Ahrens, L. H. *Geochim. Cosmochim. Acta* **1952**, *2*, 155.

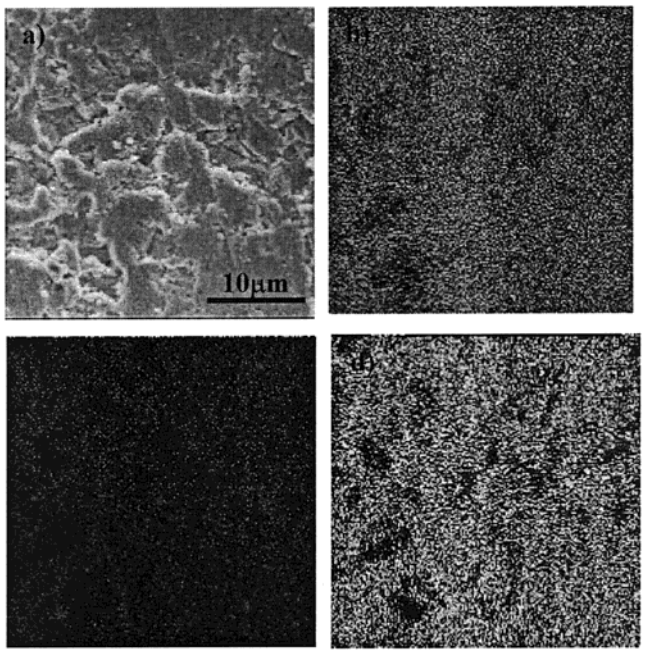

Figure 10. SEM photograph and X-ray image of the Lα line of La and Ge and the Kα line of Sr of $La_{1.5}Sr_{0.17}GeO_{5-\delta}$: (a) SEM photograph; (b) X-ray image of the La Lα line; (c) X-ray image of the Ge Lα line; and (d) X-ray image of the Sr Kα line.

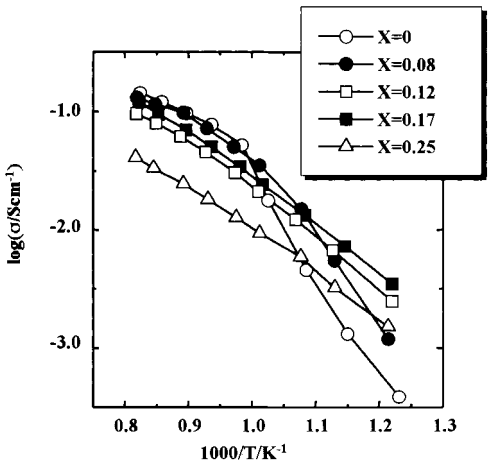

Figure 11. Arrhenius plots of La_2GeO_5-based oxide doped with Sr for the La site in $P_{O_2} = 10^{-5}$ atm.

formation of secondary phase or separation of Sr was negligible in the resultant specimens.

Figure 11 shows Arrhenius plots of La_2GeO_5–based oxide doped with Sr for the La site. It is clear that the oxide ionic conductivity was strongly affected by doping Sr for the La site. The oxide ionic conductivity at high temperature decreased but that at low temperature increased by doping Sr for the La site in La_2GeO_5. This was explained by the disappearance of the knee in Arrhenius plots of the oxide ion conductivity by doping Sr. As discussed earlier, the knee in the Arrhenius plots of La_2GeO_5-based oxide seems to appear by order−disorder transformation of the oxygen vacancy structure. Doping a small amount of Sr might stabilize the oxygen disorder structure at high to low temperature. It is clear that the oxide ionic conductivity at low temperature increased with an increasing amount of Sr and the maximum oxide ionic conductivity was obtained for the Sr concentration of 0.17 mol %. On the other hand, the oxide ionic conductivity at high temperature slightly decreased by doping Sr; however, it was almost independent

of the Sr amount. At present, a detailed mechanism for decreased oxide ionic conductivity by Sr at high temperature was not clear. However, introduction of an excess amount of oxygen vacancy generally decreases the oxide ion conductivity by the formation of oxygen vacancy and dopant cluster. Therefore, doping Sr is effective for stabilizing the high-temperature oxygen disordered structure; however, the amount of oxygen vacancy might be excess with doping Sr, resulting in a decrease in the oxide ion conductivity at high temperature.

The total conductivity of the Sr-doped sample was also independent of oxygen partial pressure from $P_{O_2} = 1$ to 10^{-19} atm, which is the same as that of La-deficient La_2GeO_5 oxide. Therefore, it is expected that the oxide ion conductivity was stably sustained in a wide P_{O_2} range from 1 to 10^{-19} atm. Figure 8 shows the temperature dependence of the transport number of oxide ion by using the electromotive forces in the H_2-O_2 and N_2-O_2 gas concentration cell. Here, it is also obvious that almost all the theoretical electromotive forces were exhibited on the N_2-O_2 and H_2-O_2 gas concentration cell using the Sr-doped sample. Therefore, oxide ion conductivity is also dominant in Sr-doped La_2GeO_5-based oxide. The oxide ion conductivity of $La_{1.5}Sr_{0.17}GeO_{5-\delta}$ was also shown in Figure 9 as a function of temperature. It should be noted that the change in slope in the Arrhenius plot was not observed on the plot of the Sr-doped specimen. Consequently a high overall oxide ion conductivity was achieved for this material in the examined temperature range. The oxide ion conductivity is slightly smaller than that of GDC and LSGM; however, oxide ion conductivity of $La_{1.5}Sr_{0.17}GeO_{5-\delta}$ was higher than that of YSZ in the whole temperature range. In addition, oxide ion conductivity was stably sustained in a wide P_{O_2} range, i.e., from $P_{O_2} = 1$ to 10^{-21} atm, which is the most attractive property of this new oxide ion conductor. Considering the near unity oxide ion transport number over a wide range of oxygen partial pressures ($1 > P_{O_2} > 10^{-19}$ atm), $La_{1.5}Sr_{0.17}GeO_{5-\delta}$ is a really new but highly attractive fast oxide ion conductor.

Conclusion

Despite the large anisotropy in crystal structure, monoclinic La_2GeO_5-based oxides exhibited the large oxide ion conductivity over a wide range of oxygen partial pressure ($1 > P_{O_2} > 10^{-19}$ atm). Except for the bismuth-based oxide, so-called BIMEVOX, this La_2GeO_5-based oxide is the first case of the oxide exhibiting high oxide ion conductivity with a low-symmetric structure, in particular, the first case of a high oxide ion conductor over a wide P_{O_2} range. Oxide ion conductivity increased by increasing the amount of oxygen vacancy, which was introduced by the La deficiency or substitution with the lower valence cation of Sr^{2+} for the La^{3+} site. The highest oxide ion conductivity at high temperature was obtained at the composition of $La_{1.61}GeO_{5-\delta}$ among the investigated La_2GeO_5-based oxide. The transport number of the oxide ion in this oxide was almost unity and the oxide ionic conductivity was as high as $\log(\sigma/\mathrm{S\ cm^{-1}}) = -0.7$ at 1223 K, which is a similar value to that of the well-known fast oxide ion conductor of Gd-doped CeO_2 or $La_{0.9}Sr_{0.1}Ga_{0.8}Mg_{0.2}O_3$. On the other hand, doping a small amount of Sr is effective for increasing the oxide ion conductivity at low temperature, albeit a decrease in the oxide ion conductivity at high temperature. Disappearance of the knee in the Arrhenius plot of the oxide ionic conductivity by doping Sr^{2+} might be achieved by stabilizing the high-temperature crystal structure to low temperature. Since large anisotropy in oxide ion conductivity was expected, it is further anticipated that the oxide ion conductivity would be improved by making a single crystal of this La_2GeO_5-based oxide. As a result, it can be concluded that La_2GeO_5-based oxide materials may open up a new frontier in obtaining a high oxide ion conduction.

Acknowledgment. The authors acknowledge the financial support from a grant-in-aid from the Ministry of Education, Culture and Sports of Japan. Part of this study was also financially supported by the International Joint Research Program from NEDO. The crystalographic analysis by Mr. G. Fujinawa, Rigaku Co., was greatly appreciated.

JA0014537